AEROSPACE REPORT NO.
TOR-2020-01640

Geant4 Simulations of ECP-Lite Microdosimeter Response to Electrons and Protons

June 26, 2020

Mark D. Looper
Magnetospheric and Heliospheric Sciences
Space Sciences Department

Prepared for:

Space and Missile Systems Center
Air Force Space Command
483 N. Aviation Blvd.
El Segundo, CA 90245-2808

Contract No. FA8802-19-C-0001

Authorized by: Defense Systems Group

Acknowledgments

The author acknowledges discussions with Can Nguyen, Tim Guild, Bill Crain, Joe Mazur, and other members of the ECP-Lite team.

Abstract

The ECP-Lite compact sensor package includes six microdosimeters, as well as a Faraday cup plasma analyzer and a surface-charging monitor. We have used the Geant4 open-source Monte Carlo radiation-transport toolkit to model the response of the microdosimeters to electrons and protons, which will dominate the radiation environment that they will measure in space. The ECP-Lite housing is made of aluminum walls at least 300 mils thick, except where the sensors view space through windows providing reduced shielding; this was found to be very effective in rejecting dose from penetrating particles, so that the microdosimeters will mainly respond to particles entering their apertures through the well-characterized shielding under which they are placed, rather than to particles penetrating varying amounts of shielding to the sides or the rear of the instrument.

Contents

Figures

Tables

1. ECP-Lite Configuration

1.1 Sensor Layout

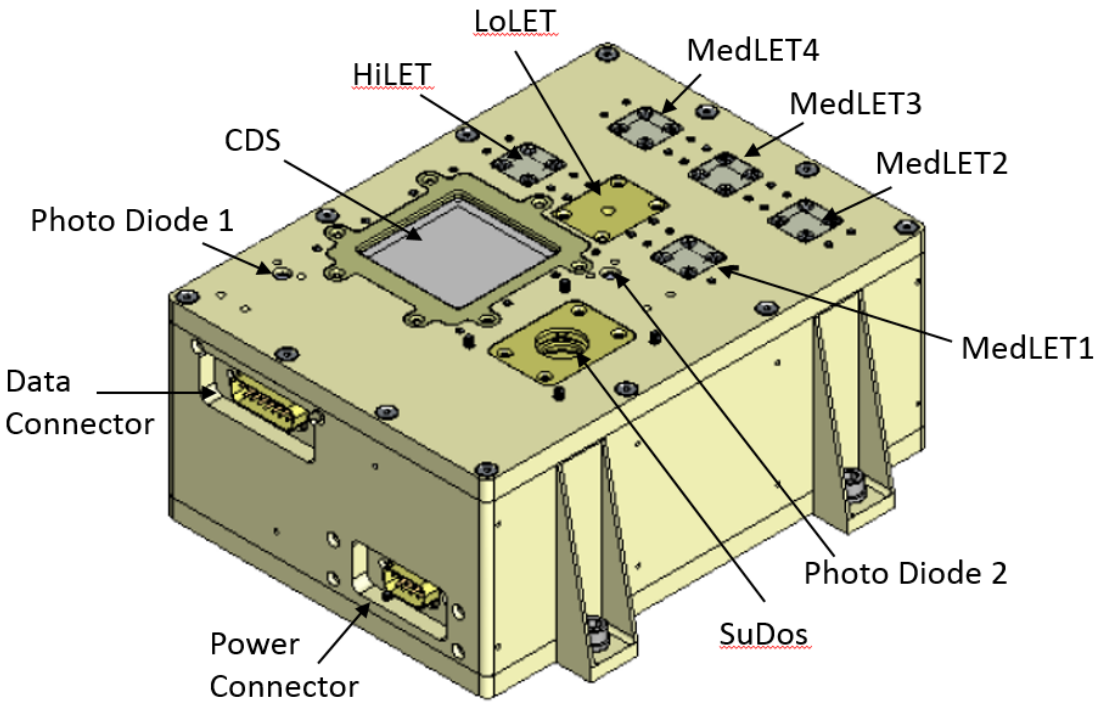

Figure 1. Locations of sensors atop ECP-Lite, from FM2 pre-ship review charts.

Figure 1 is a diagram of the entire ECP-Lite instrument with its constituent sensors and other components labeled, from a slide in the FM2 pre-ship review chart package. Six of the eight radiation-environment sensors are variants of the NuDos microdosimeter; SuDos measures the low-energy particles that cause surface charging, and CDS measures the resultant surface charging and any electrostatic discharges that result. Characterization of response of SuDos and CDS requires tools other than the Geant4 software used in this work, and they are not analyzed further herein.

The MedLET and HiLET sensors are physically identical, with the only difference being that the electronic threshold, which is required to be exceeded in order for a given particle's energy deposit to be tallied as radiation dose, is higher for HiLET in order to reject electrons and isolate the dose due to protons (and heavier ions, if present), as shown in Table 1. Each MedLET and HiLET microdosimeter has a detector consisting of a silicon chip 7 mm x 3 mm x 250 μm; the LoLET unit has a circular detector 1.8 mm in diameter x 60 μm thick mounted in an identical housing. The MedLET and HiLET microdosimeters are exposed to space under aluminum shields attached to the outside of the instrument, with varying thicknesses as specified in Table 1, while the LoLET unit is behind a thin aluminum foil that views space through the hole visible in Figure 1.

Table 1. Parameters of Microdosimeters, Typical of FM 2 to 7

Microdosimeter	Electronic threshold	Aluminum window thickness
LoLET	50 keV	7 μm foil
MedLET1	100 keV	2.6 mils
MedLET2	100 keV	13 mils
MedLET3	100 keV	30 mils
MedLET4	100 keV	50 mils
HiLET	1 MeV	32 mils

1.2 Reference Documents Used

Table 2 lists the main documents used to characterize the geometry of the sensors and the surrounding inert material for this work, and such other determinants of response as electronic thresholds, window thickness, etc. Numerous questions were also answered via personal emails from other ECP-Lite team members.

Table 2. Primary Documents Used for Reference

Filename	Description	Used In This Report For
ECPL-04003 Sensor Assembly 14April2020.EASM	eDrawing of entire instrument box	Bulk geometry and dimensions
Nu uDosimeter 5Jan2017.EASM	eDrawing of microdosimeter unit	Geometry and dimensions of detectors and mounting
ECPL-00001-C ICD w-ECR 144 – signed.pdf	Interface Control Document	Electronic thresholds, window thicknesses
ECP-Lite FM2 Pre-Ship Review_2020_0325.pptx	Charts from Pre-Ship Review	Host mounting, labeling of detectors (Figure 1 above)

2. Setup of Simulations

2.1 The Geant4 Code Package

To model the response to electrons and protons of the ECP-Lite microdosimeters, we used version 10.5 of the Geant4 open-source Monte Carlo radiation-transport toolkit [1], running on Aerospace's High Performance Computing Linux computer clusters. This software enables users to simulate the transport of arbitrary energetic particles through a 3-D user-defined geometry, with full access to all properties of the particles as they travel. By means of this, we can tabulate energy deposit in sensitive parts, like the detector chips of the microdosimeters, with realistic representations of the full physics, including electromagnetic and nuclear interactions, production and tracking of secondary energetic particles, and stochastic processes like scattering and energy-deposit fluctuations. (For the record, we used reference physics list Shielding_EMZ.). The geometry can be imported from CAD files in the STEP format, but the code runs much faster if it is instead built by hand in C++ from simple substructures (boxes, cylinders, etc.), as we did for these simulations. This section shows the geometry as used in the simulation, which was based on the eDrawing files listed in Table 2.

2.2 Geometry of Sensor Plate

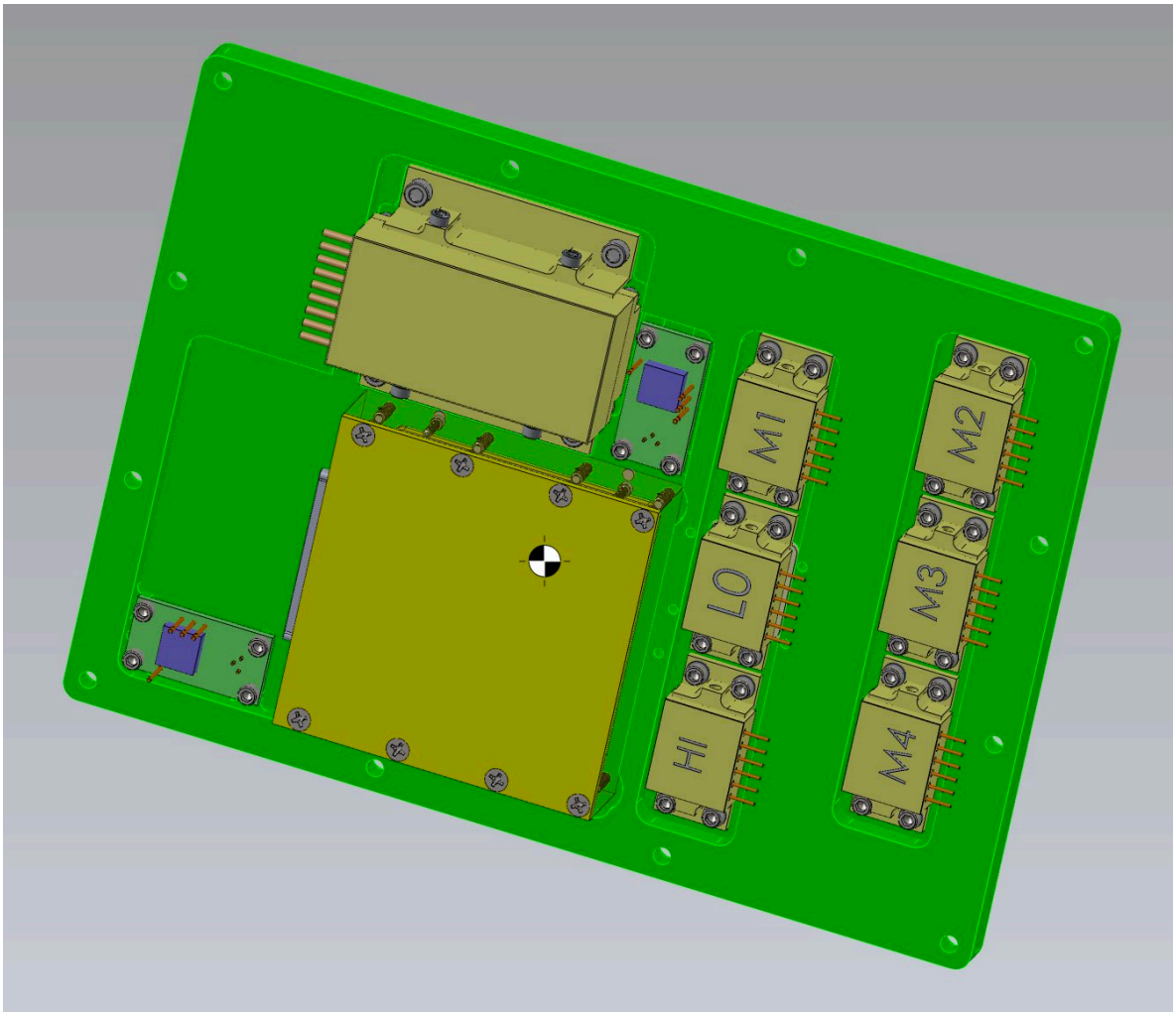

Figure 2. Underside of sensor plate, as represented in the CAD file.

The top lid seen in the diagram in Figure 1 is referred to as the "sensor plate." It is made of aluminum 300 mils thick, with hollows underneath and holes through to mount the energetic-particle sensors and two photodiodes (not simulated here). Figure 2 shows the underside of this plate, in a screenshot from the CAD file listed in the first line of Table 2.

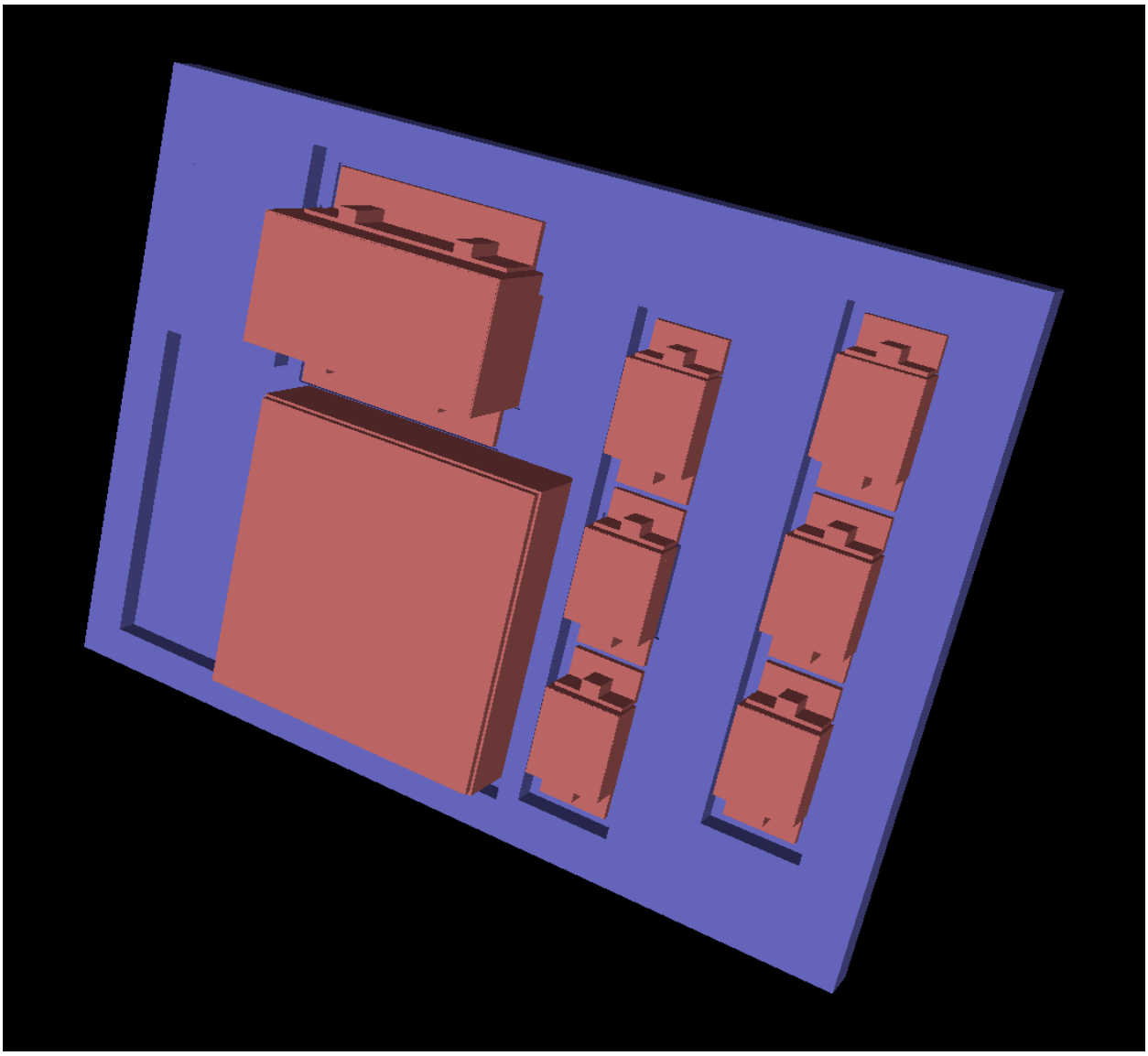

Figure 3. Underside of sensor plate, as represented in Geant4.

Figure 3 also shows the underside of the sensor plate, this time in a screenshot of a VRML2 geometry dump created by the Geant4 code. Different materials are represented by different colors here, with aluminum in blue and Kovar in red. The six NuDos microdosimeters are at the right, and SuDos and CDS are the larger boxes at left.

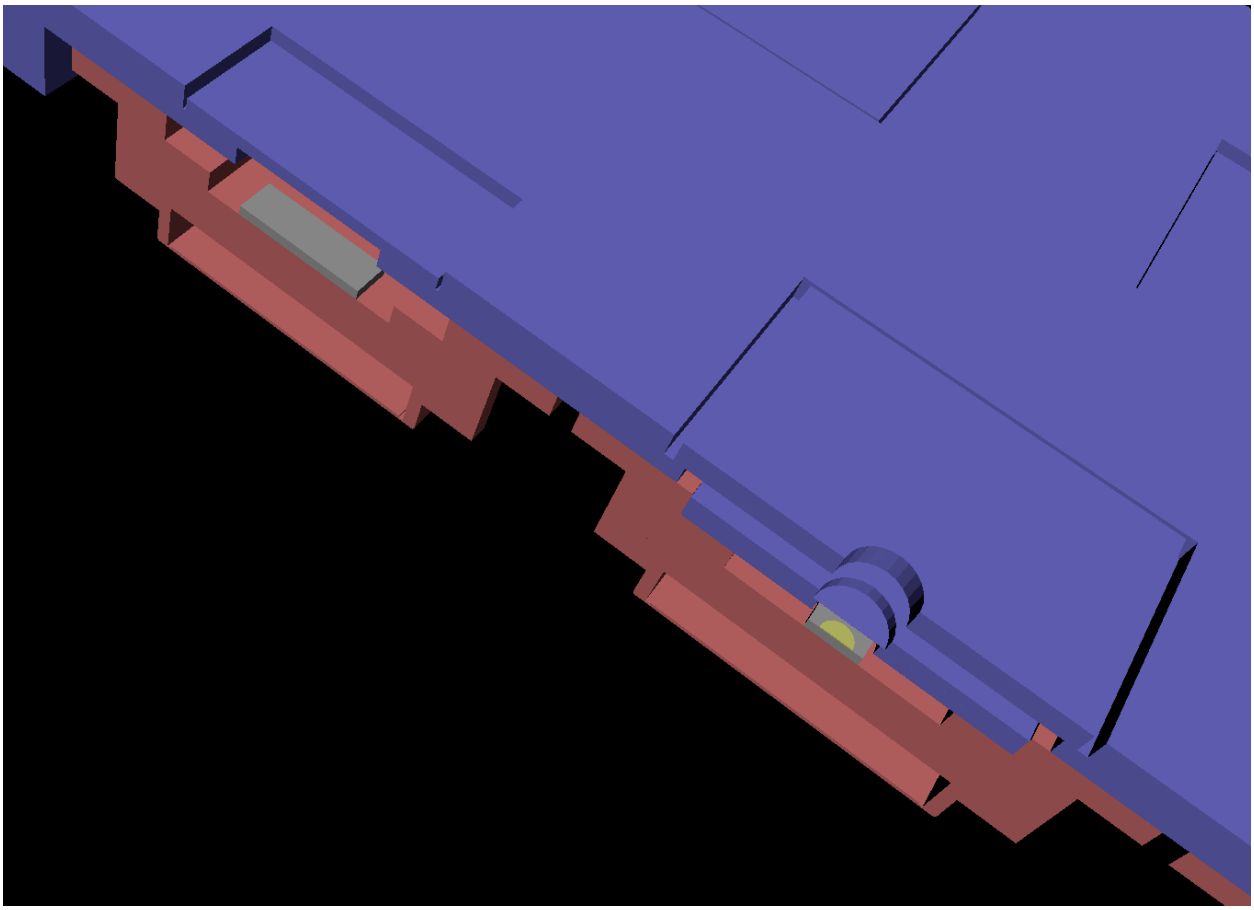

Figure 4. Section through the middle of the circular LoLET detector, with HiLET to the left, from the Geant4 geometry.

Figure 4 shows a cutaway section of two of the microdosimeters from the Geant4 geometry, showing the inside of the Kovar enclosures, the alumina detector pedestals (light gray), and the circular LoLET silicon detector (yellow) at the right, through the center of which the cut was made. The foil above this detector, its holder, and the cover above with hole through it to expose the foil to space are shown. For HiLET, shown at left, the section missed showing the detector, but it displays the 32 mil aluminum window through which that detector views space. During the simulations, energy deposits in the six detectors of the microdosimeters were tallied; the SuDos and CDS housings were modeled in comparable detail, but were only considered as inert shielding for the microdosimeters.

2.3 Balance of Geometry

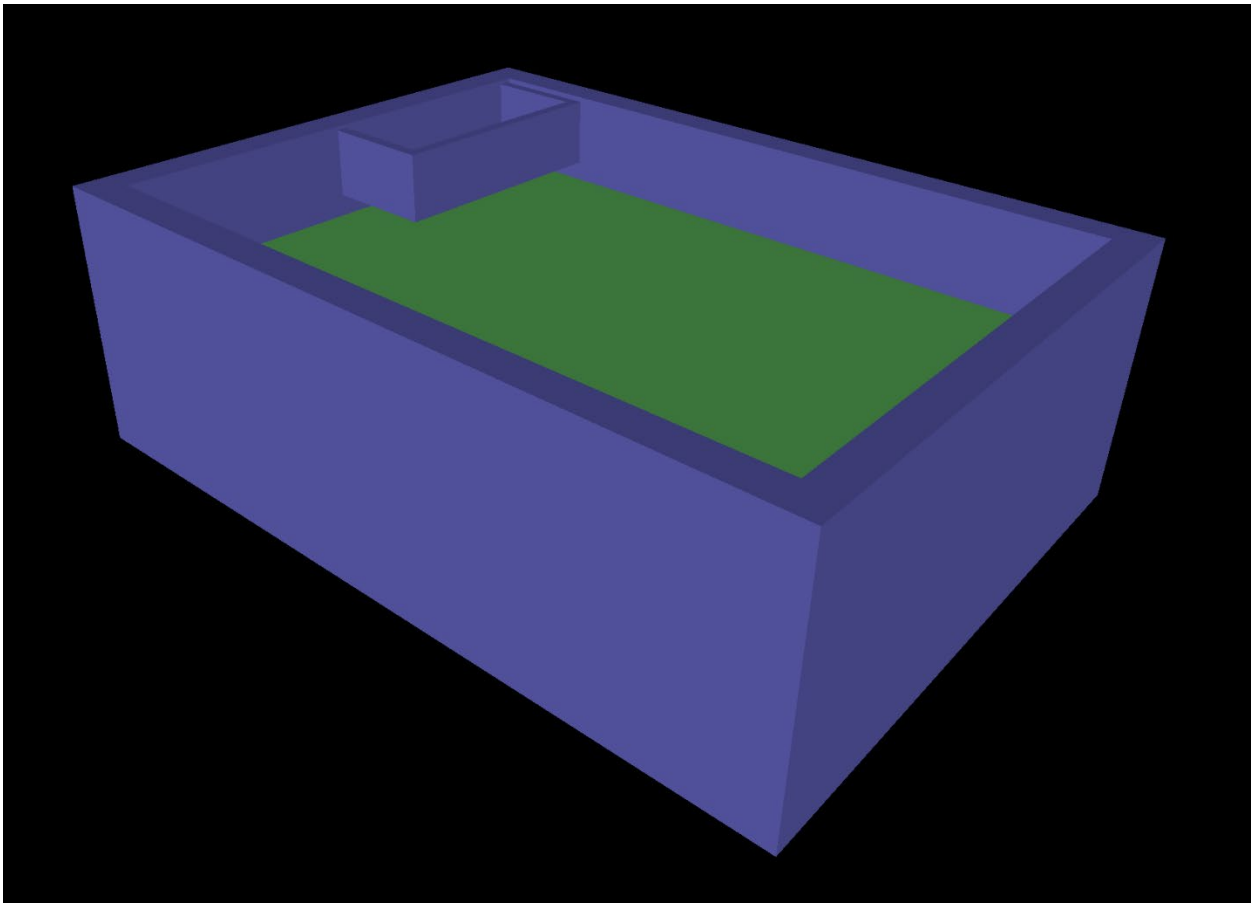

Figure 5. View of the main electronics box, from the Geant4 geometry.

Figure 5 shows the box with the sensor plate removed. A simulation of radiation dose needs to model in detail the distribution of inert material close to the sensitive detectors, but as distance from them increases only the bulk distribution of mass is needed. Thus the remainder of the model was geometrically more simplified than that of the sensor plate, with the 300 mil aluminum walls of the box, a 100 mil aluminum divider in the middle with a printed-circuit board (green) on either side, and two small aluminum internal boxes that mount or shield various components (one shown at far corner of Figure 5). There was also a 300 mil aluminum lid on the bottom of the box.

3. Geant4 Results

3.1 Subdividing Response by Primary Particle Trajectories

To simulate the response of each microdosimeter to incident protons and electrons, the entire box was illuminated in turn by isotropic, monoenergetic fluxes of each species ranging from 30 keV to 10 MeV for electrons and 300 keV to 3 GeV for protons. Energy deposits in the six silicon detectors were tabulated, and logged along with the species, energy, incidence direction, and starting location on the surface of the box of the causative incident particle. For a given unit-vector direction $\hat{v}$ and energy E, the directional dose response function $R(E, \hat{v})$ for each detector has dimensions of dose x area, for example rad cm^2, and for a planar flux of particles F per unit area per second from that direction, the dose rate in that detector will be FR. If we have an isotropic flux $j(E)$ with units of (cm^2 sr sec MeV)$^{-1}$, we can integrate the directional response over the full 4π solid angle to get an omnidirectional dose response $\mathcal{R}(E)$ in units of rad cm^2 sr, and the dose rate will be $\int \mathcal{R}(E)j(E)dE$. These two quantities, the directional dose response $R(E, \hat{v})$ and the omnidirectional dose response $\mathcal{R}(E)$, are what is plotted in the figures later in this section.

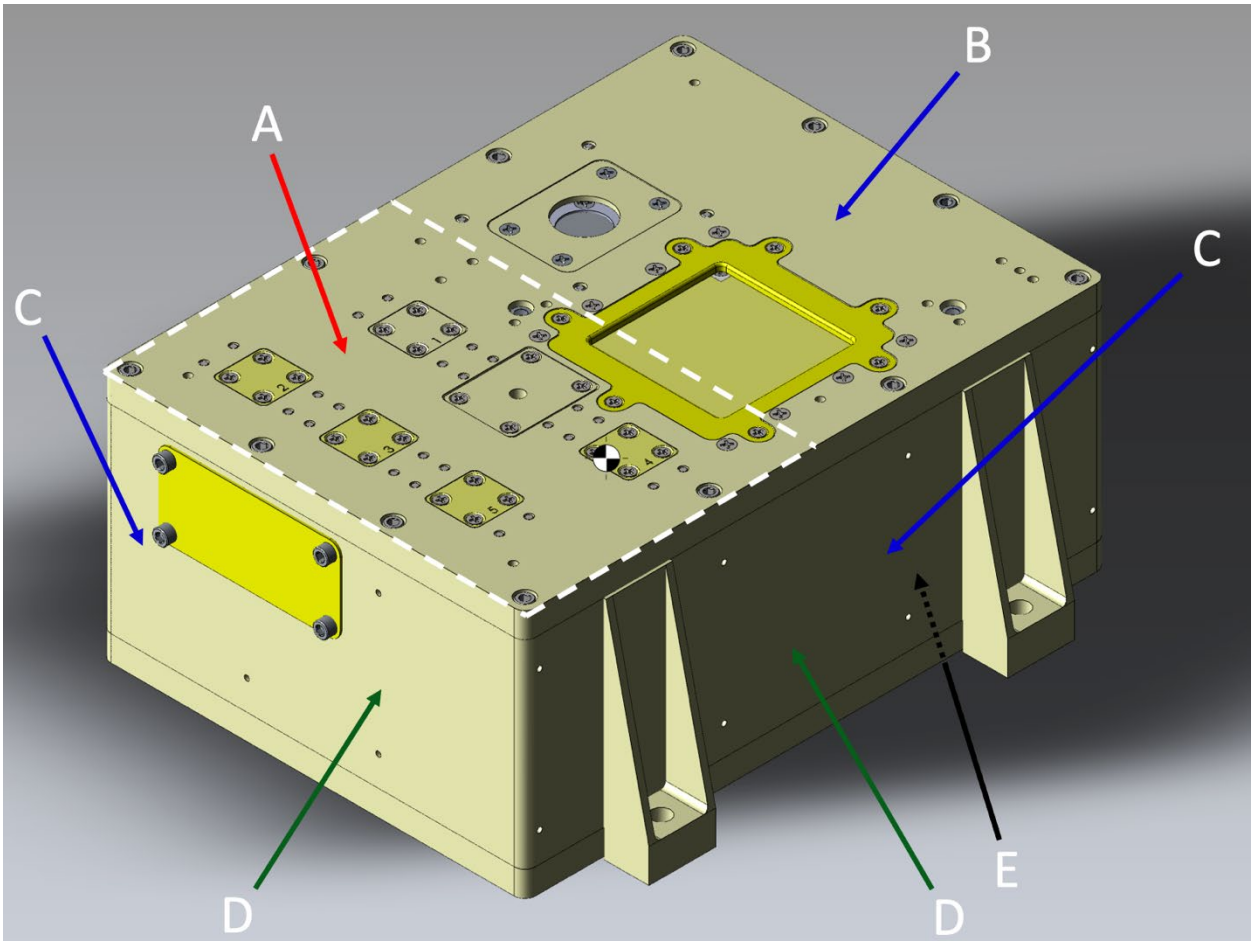

Figure 6. Image of ECP-Lite instrument from the CAD file, with labeled arrows showing subsets of the simulated particle trajectories composing different parts of the responses reported below.

Because we keep track of the position and direction of simulated particles as well as their energy, we can separate the dose responses according to these parameters. Figure 6 shows the four subsets called out in

the figures below, with colored and labeled arrows representing different categories of incident-particle trajectories. The red arrow A indicates the main response, with particles arriving from above and striking the half of the top plane that encompasses the apertures of the microdosimeters, indicated by the white dashed lines. The blue arrows also represent particles arriving from above, with the arrow B indicating particles striking the other half of the top plate and the arrows C representing particles striking the four sides of the box from above; these are combined into the "secondary (down)" response in the plots to follow. Green arrows D indicate the "secondary (up)" response to particles striking the sides from below, and finally the black arrow E represents particles coming from below to strike the bottom of the box. The utility of this is that, for example, if an ECP-Lite unit is mounted on a large spacecraft that blocks all particles arriving from below (except possibly the extremely penetrating galactic cosmic rays), then we can ignore any dose that might result from particles in the "secondary (up)" or "bottom" subsets as they would have had to penetrate the whole spacecraft to reach ECP-Lite.

A final advantage of tracking position and energy is that we can, separately, run simulations of particles coming only into the area around the microdosimeters (the "main" response) to boost statistics for this portion of the simulated response, and then average it with the omnidirectional response with appropriate weighting. Since the area enclosed by the dashed white line is about 1/8 of the entire surface area of the box, simulating a number of particles incident there that is equal to the number in the main simulations illuminating the whole box will boost statistics there by a factor of about 9. This is done, and the two sets of calculations folded together, in the results presented below.

3.2 Electron Dose Response

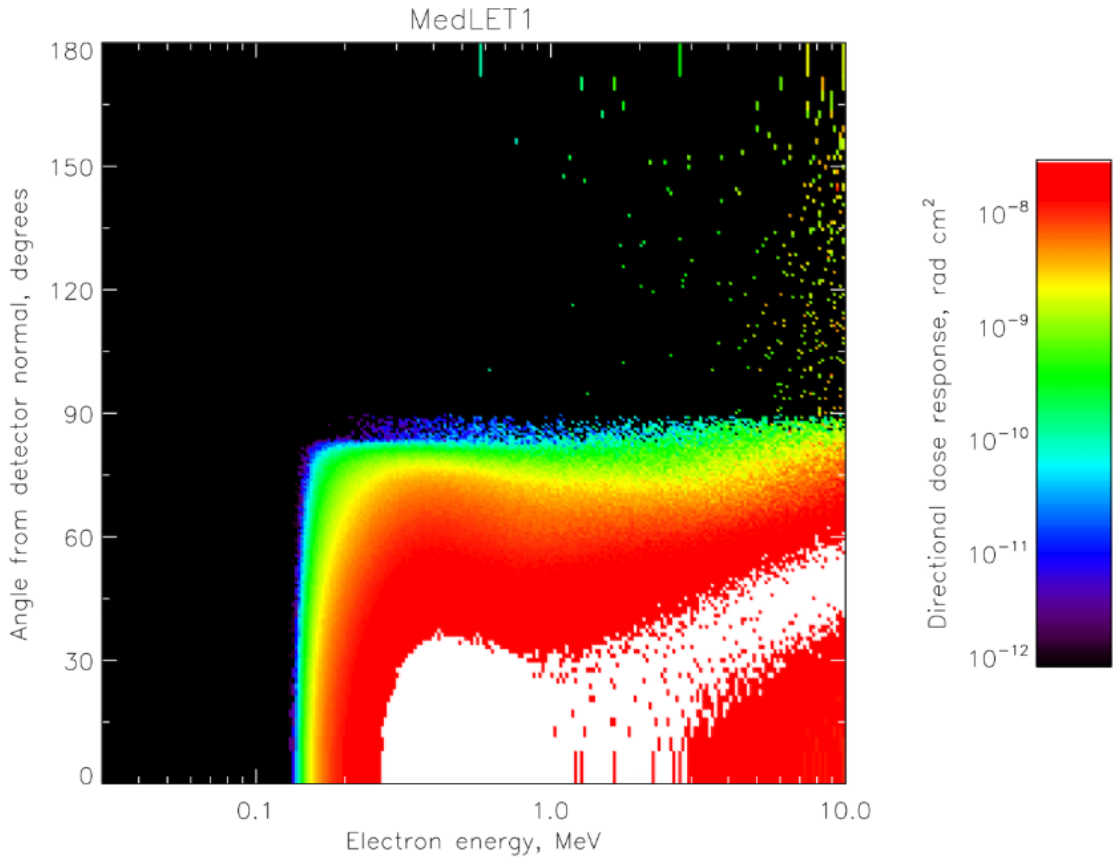

Figure 7. Directional dose response of MedLET1 microdosimeter to electrons as a function of energy and angle off of detector normal. In this and all subsequent colorscale plots, white indicates saturation of the colorbar past red.

Figure 7 shows the directional dose response $R(E, \hat{v})$ of the MedLET1 microdosimeter to electrons. The response is not cylindrically symmetric as it would be for a stack of circular detectors and apertures, say, but the directions have been averaged in azimuth about the detector normal for this plot, to give a sense of where the particles contributing to the response are coming from. The response is well-constrained to the half of directions coming down from above the detector apertures, indicating that the minimum of 300 mils of aluminum wall to the rear is effectively shielding against background from penetrating electrons up to the highest energy simulated, 10 MeV. The fact that the band of strong response does not widen in angle appreciably as energy increases indicates that there are no substantial thin spots in the shielding around the aperture window that start to be penetrated as energies increase, though a slight enhancement around 1 MeV in the 80°-90° range suggests that a small amount of such penetration occurs.

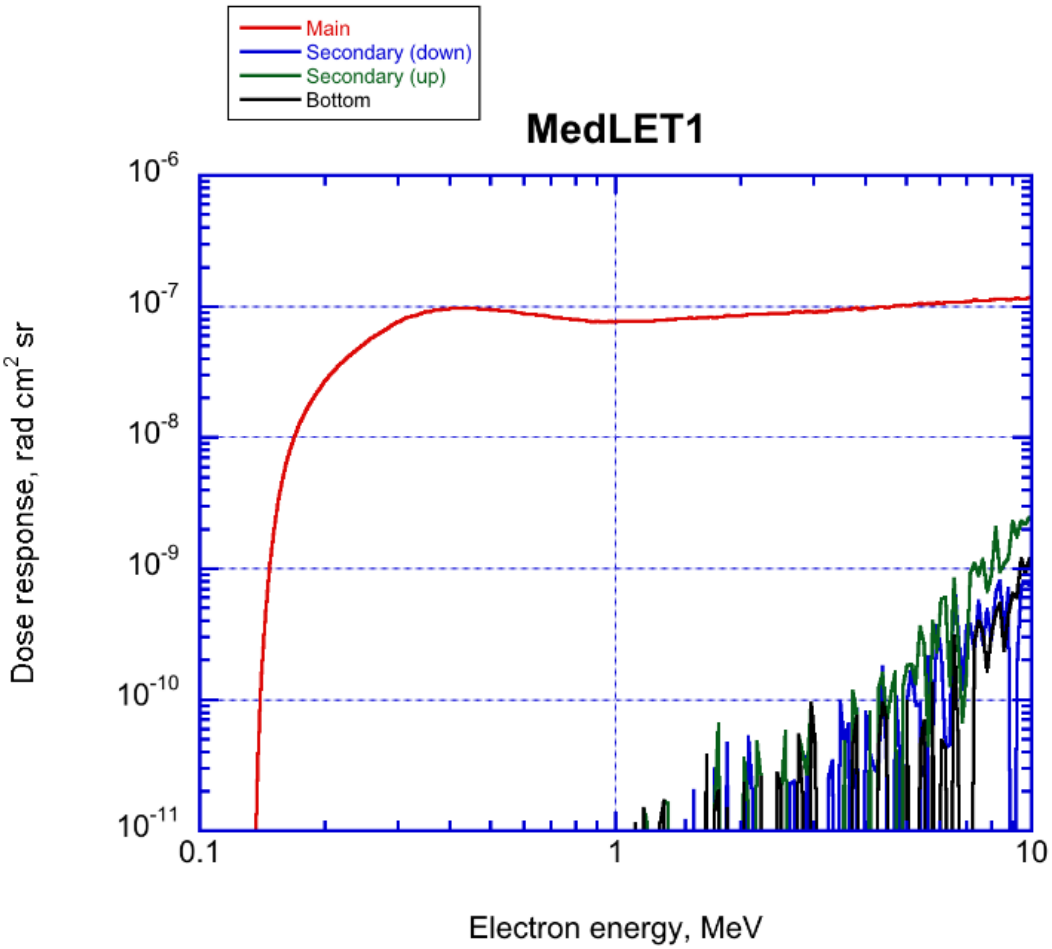

Figure 8. Omnidirectional dose response of MedLET1 to electrons, subdivided by particle trajectories as described in Section 3.1.

Figure 8 averages over all directions to give the omnidirectional dose response $\mathcal{R}(E)$ as a function of energy for electrons into MedLET1. The response is further broken down into the four categories of incident-particle trajectories as described in Section 3.1. This plot quantifies the effectiveness of the walls of the ECP-Lite package at shielding against penetrating electrons, in that the red "Main" response is two or more orders of magnitude above the responses to particles striking away from the microdosimeter's aperture.

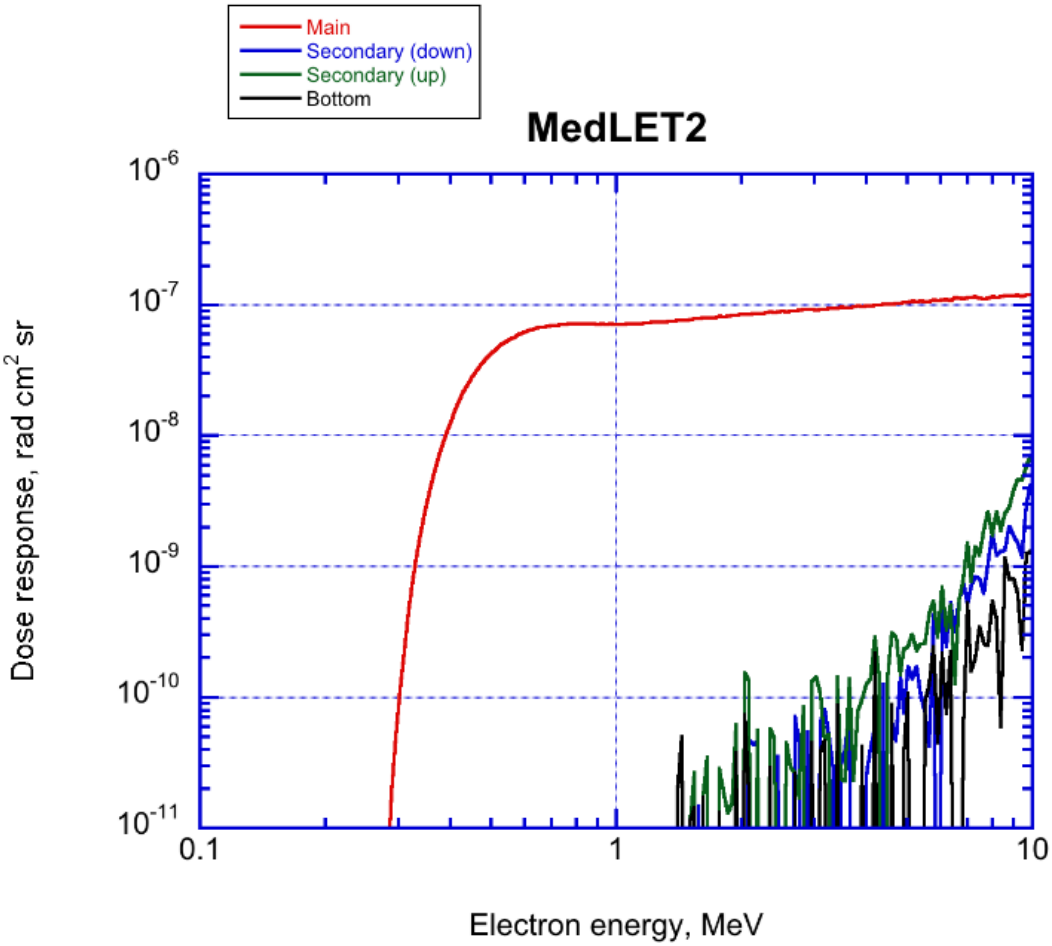

Figure 9. Omnidirectional dose response of MedLET2 to electrons.

The directional dose response plots, as in Figure 7, are qualitatively the same for the other MedLET detectors except that threshold energies increase with the thickness of the window over the aperture as listed in Table 1, so these plots will not be shown here. Figure 9 shows the omnidirectional dose response of MedLET2 to electrons. As in Figure 8 for MedLET1, the dose overwhelmingly comes in through the window over the detector.

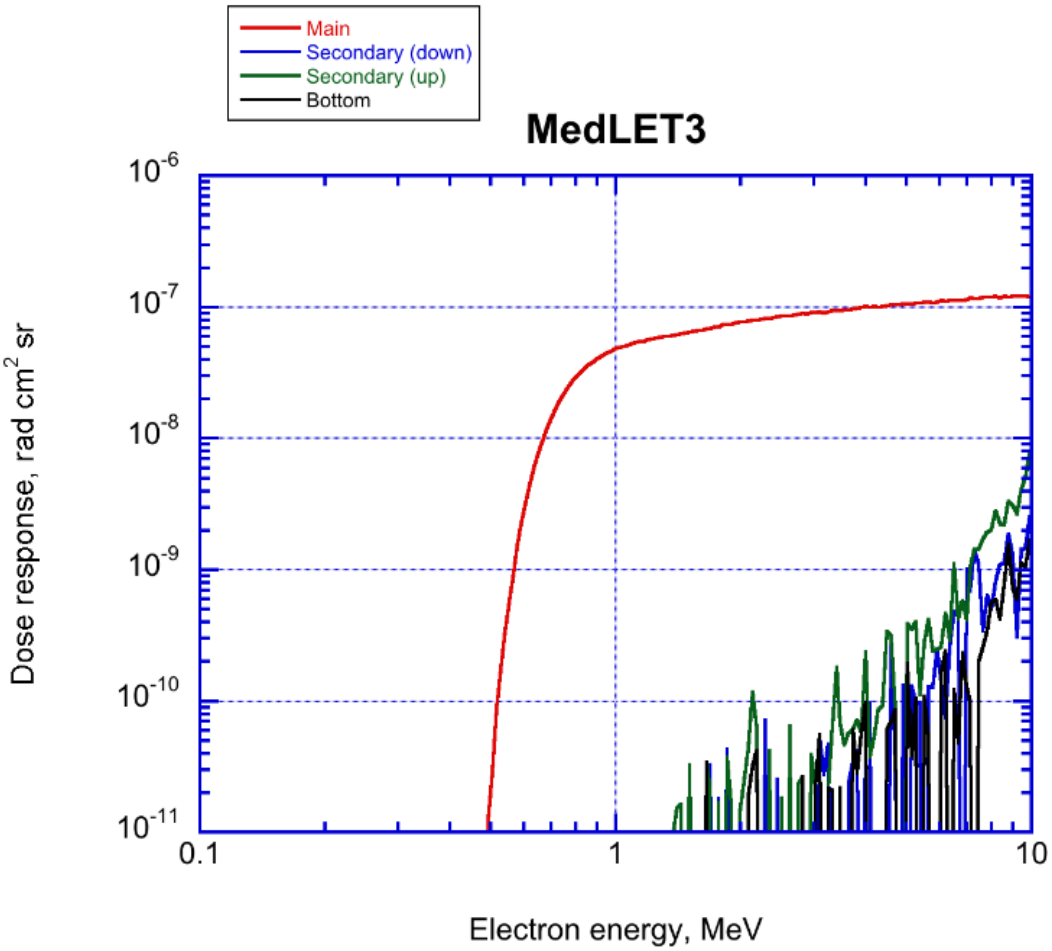

Figure 10. Omnidirectional dose response of MedLET3 to electrons.

Figure 10 shows the omnidirectional dose response of MedLET3 to electrons. Again, except for the increased threshold, the pattern of response is very similar to that of the other MedLET units.

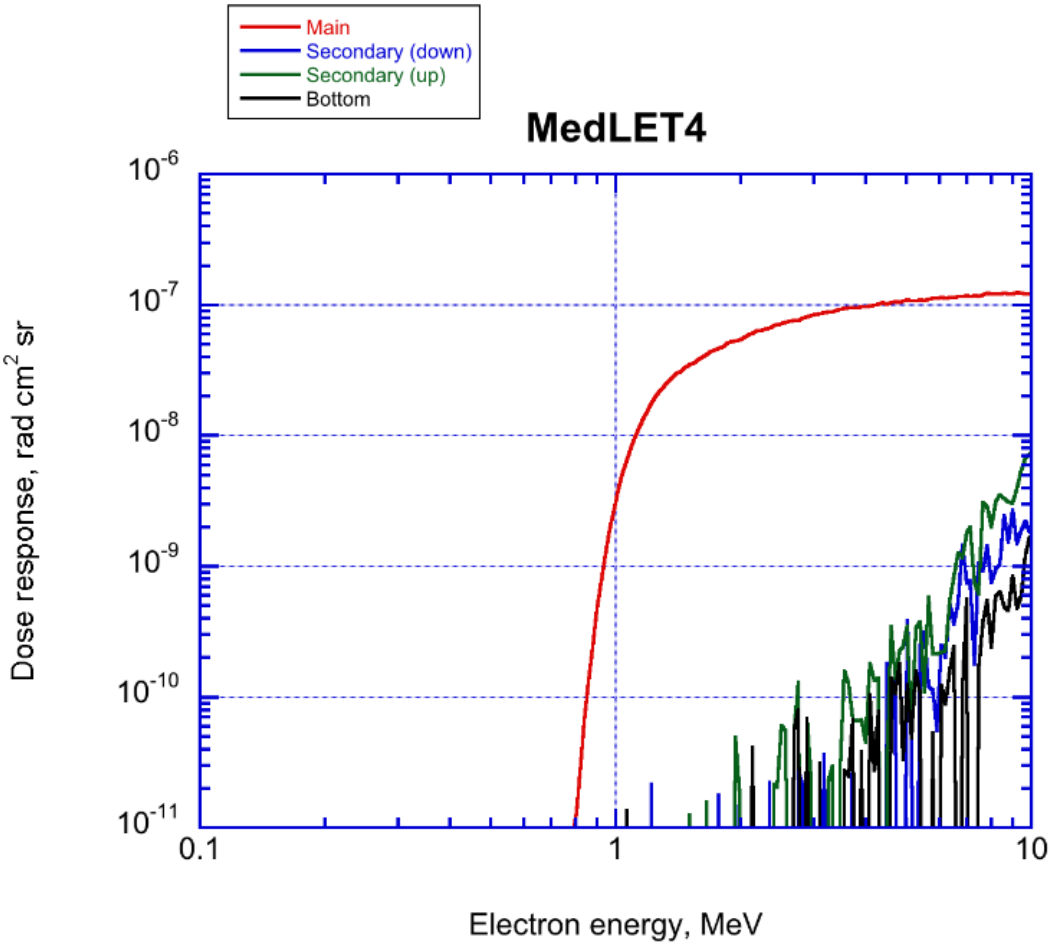

Figure 11. Omnidirectional dose response of MedLET4 to electrons.

Figure 11 shows the omnidirectional dose response to electrons for MedLET4, with the thickest window over its detector. Again, it is very similar to that of the other MedLET units.

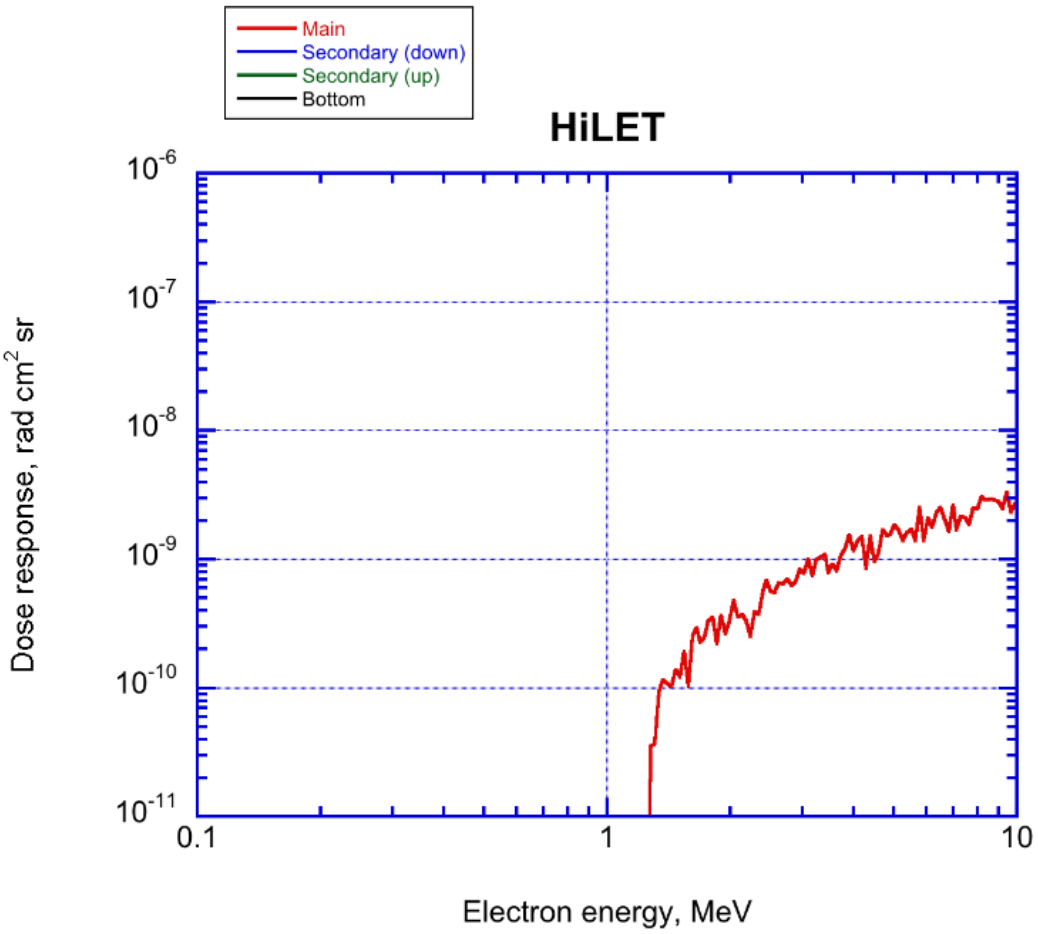

Figure 12. Omnidirectional dose response of HiLET to electrons.

HiLET has a window very close in thickness to that of MedLET3 (see Table 1), but as Figure 12 shows, its dose response is greatly suppressed by the high energy-deposit threshold.

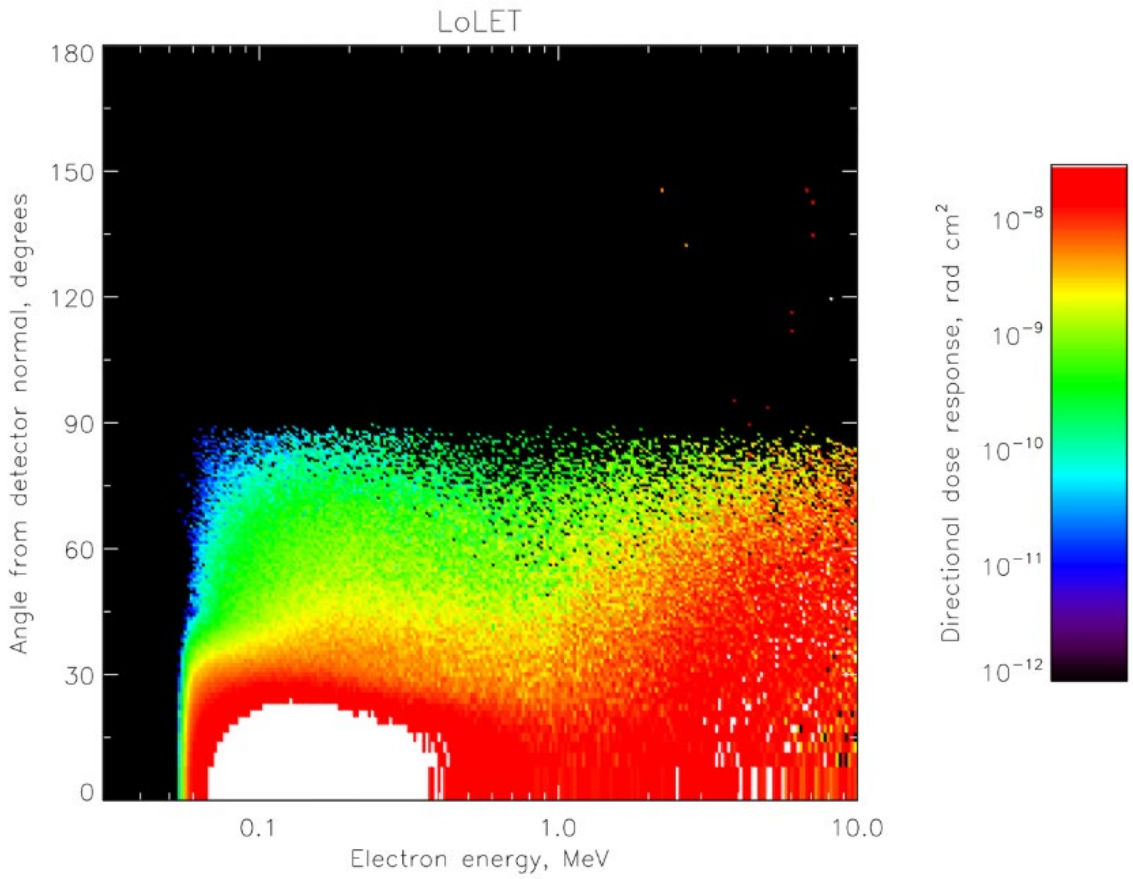

Figure 13. Directional dose response of LoLET to electrons.

Figure 13 shows the directional dose response of LoLET to electrons. The band of strong response near the threshold at about 55 keV is narrower in angle, because these particles are collimated by the circular hole in the cover, as is visible in Figure 4. There is some weak response at these low energies out to 90° due to scattering, but around 1 MeV we start to see a stronger response toward 90°. This is due to penetration of the cover around the hole and/or the holder around the foil, which even together are much thinner than the 300 mil wall covering areas away from the microdosimeters. Thus the angular pattern of dose response will only be roughly uniform up to about 1 MeV, which may be important if spectral inversions are to be done (a topic beyond the scope of this report).

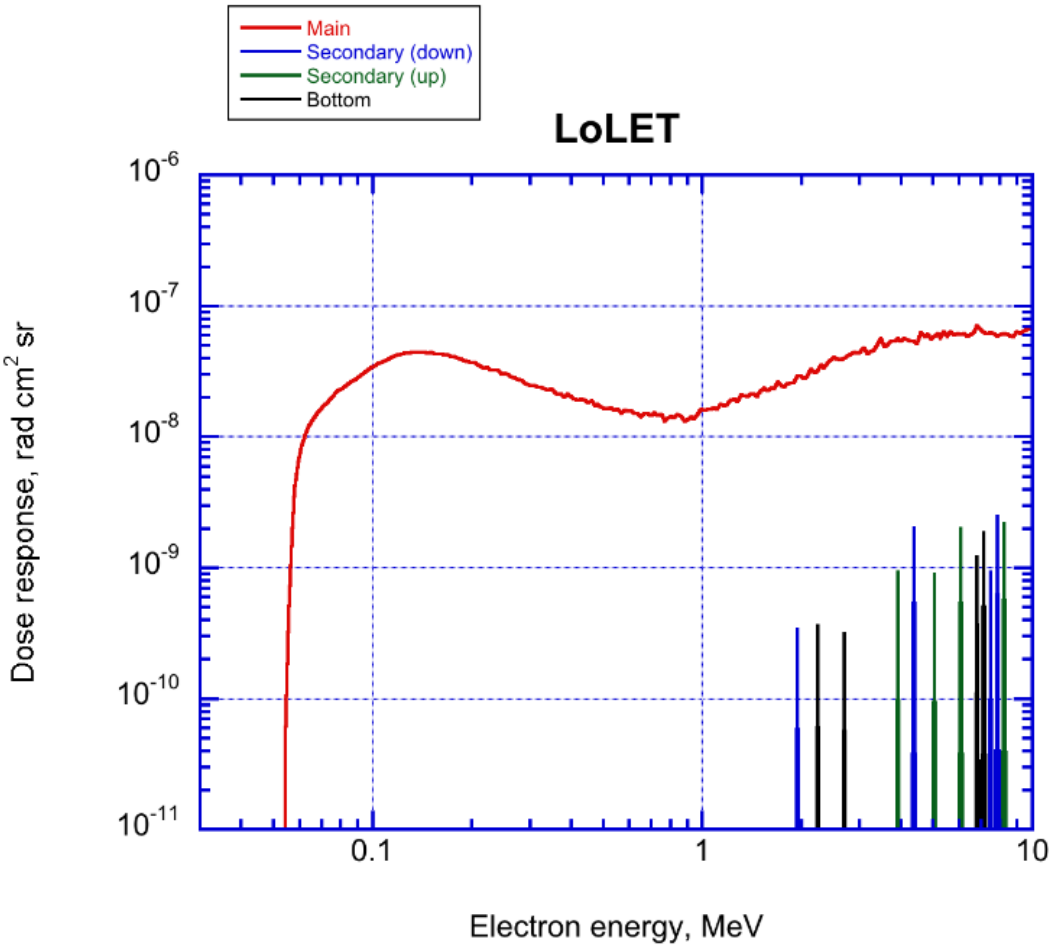

Figure 14. Omnidirectional dose response of LoLET to electrons.

Figure 14 shows the omnidirectional dose response of LoLET to electrons, which bears out the pattern in Figure 13. We see a rise from threshold until energy deposit in the detector reaches a maximum as electrons just penetrate it around 150 keV, then a falloff as more of the electron's energy is carried away by the penetrating electron, followed by a rise starting around 1 MeV as the surrounding inert material starts to be penetrated. As for all other microdosimeter units, the response away from the aperture (in this case, including the cover plate through which the aperture hole is bored) is negligible.

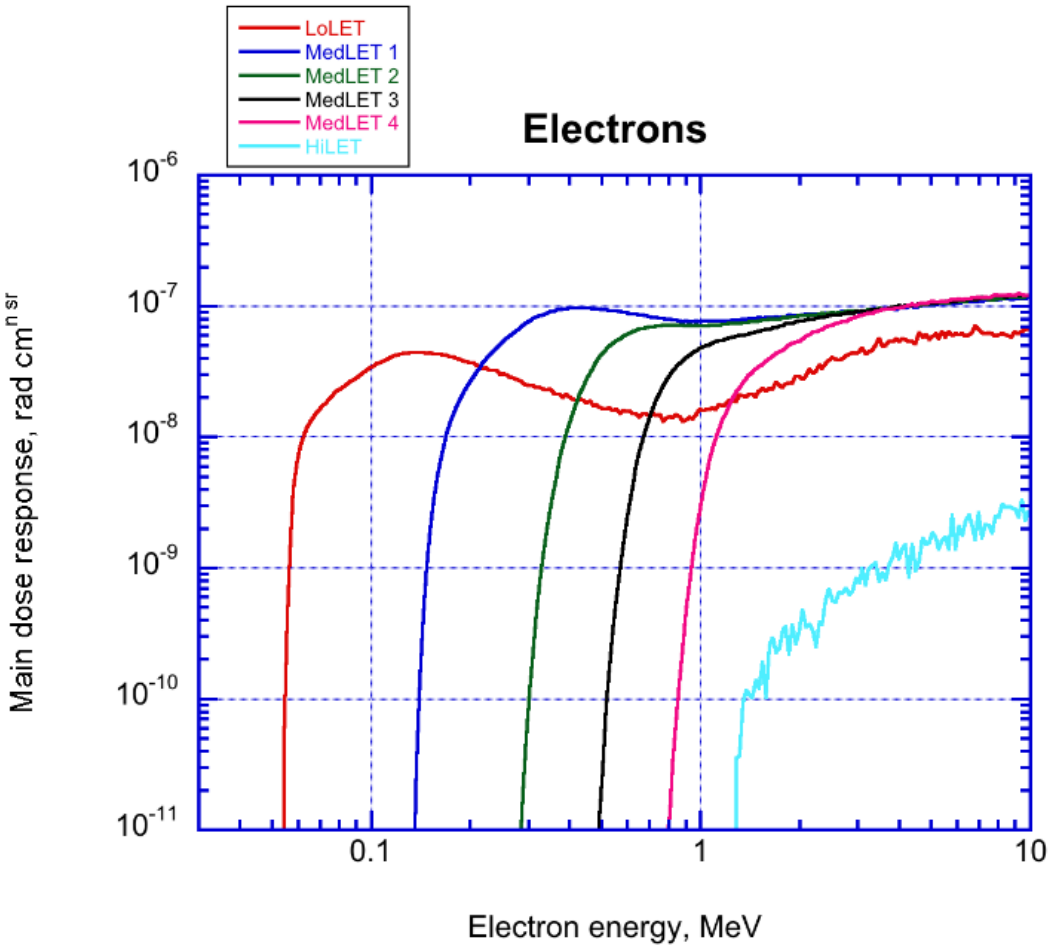

Figure 15. Omnidirectional dose response of all microdosimeter units to electrons, into and near their apertures/windows.

Figure 15 summarizes the omnidirectional dose responses to electrons of all six microdosimeter units, plotting the main response (red curves in Figures 8-12 and 14) for each. Since the response to electrons hitting away from the apertures is negligible up to 10 MeV, which is higher than electrons are commonly observed in any significant numbers in the near-Earth space environment, these response curves are unaffected by any additional shielding provided to the sides of or behind the ECP-Lite package by other hardware mounted nearby, the body of the spacecraft, etc.

3.3 Proton Dose Response

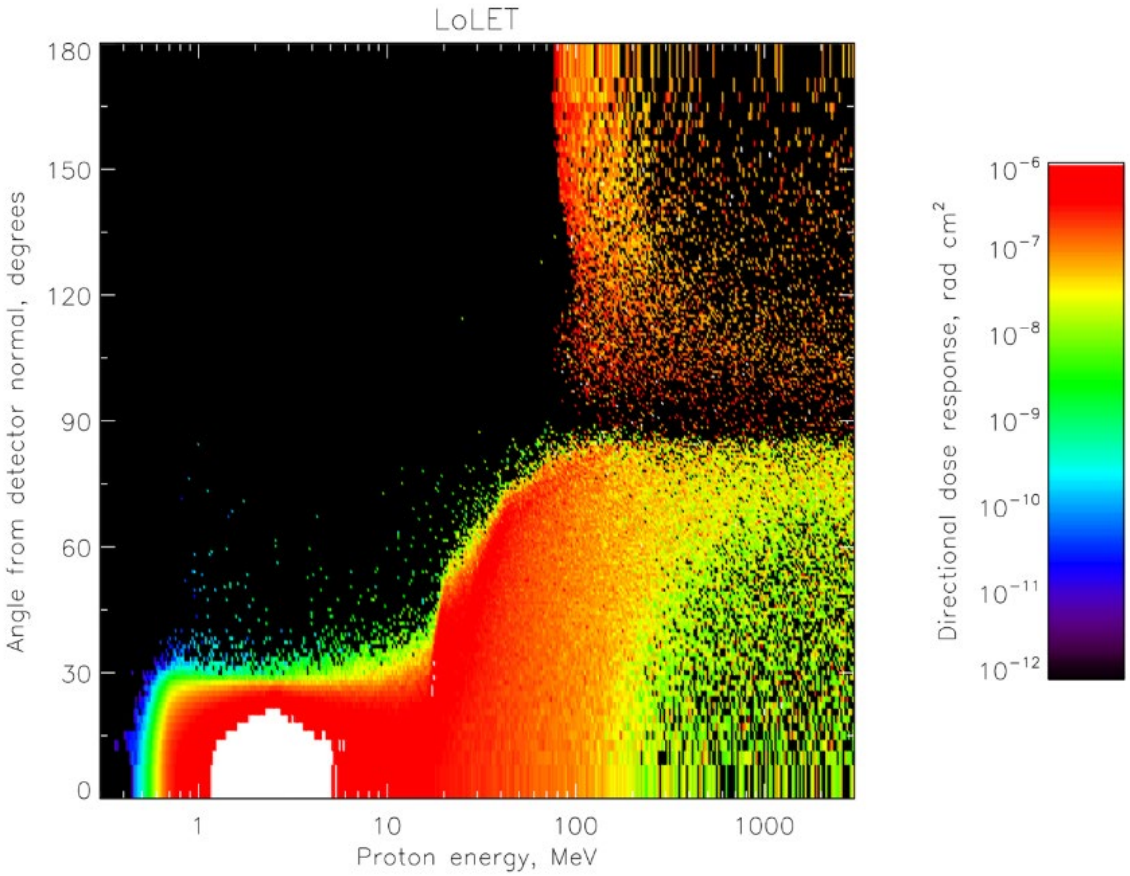

Figure 16. Directional dose response of LoLET to protons.

Figure 16 shows the directional dose response of LoLET to protons, for comparison with Figure 13 for electrons. The collimated response at low energies is more sharply cut off at about 30° here because protons scatter less than electrons. We start to see penetration of the cover outside the hole around 20 MeV, and another "shoulder" where the foil holder also starts to be penetrated at about 40 MeV. Unlike the situation for electrons, protons are able to penetrate any surface of the ECP-Lite box starting at about 80 MeV, so response out to 180° off the detector normal (through the back of the box) is seen above that energy.

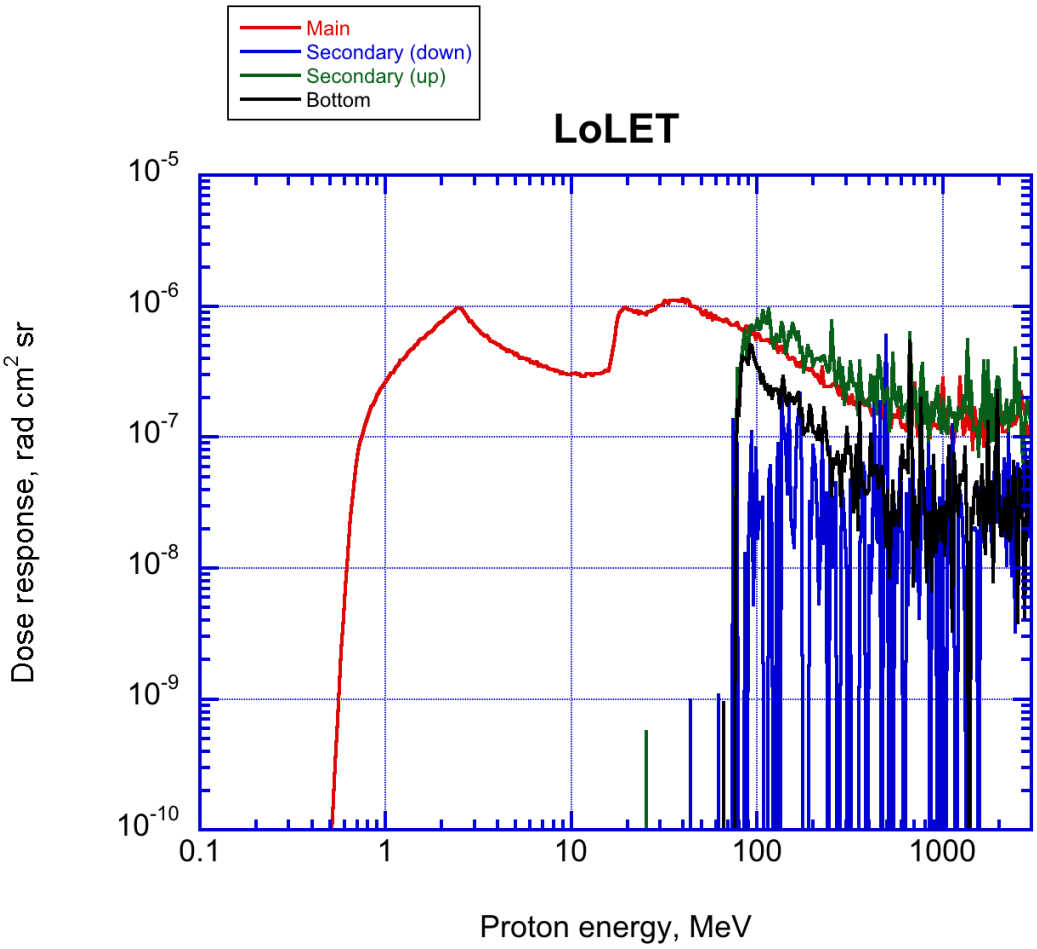

Figure 17. Omnidirectional dose response of LoLET to protons.

Figure 17 shows the omnidirectional dose response of LoLET to protons, integrating over angles in Figure 16. There are some features visible that are similar to those in the curve for electrons in Figure 14, though of course sharper because protons scatter less: a peak where protons just stop in the detector before penetrating it and thus deposit their maximum energy, around 2 MeV, followed by a falloff and then a rise where penetration of the cover begins around 20 MeV as discussed above. The penetrating background response actually exceeds the main response above about 80 MeV; however, note that the highest response is in the green and black curves, both of which will be eliminated, or at least have their threshold energies raised much higher, because the causative up-going protons would have to penetrate the spacecraft on which an ECP-Lite unit would be mounted. We only need to be concerned about the "secondary (down)" response, which is about an order of magnitude lower than the main response, and we needn't even worry about that if ECP-Lite is surrounded by other components rather than mounted on a flat outer surface of the spacecraft.

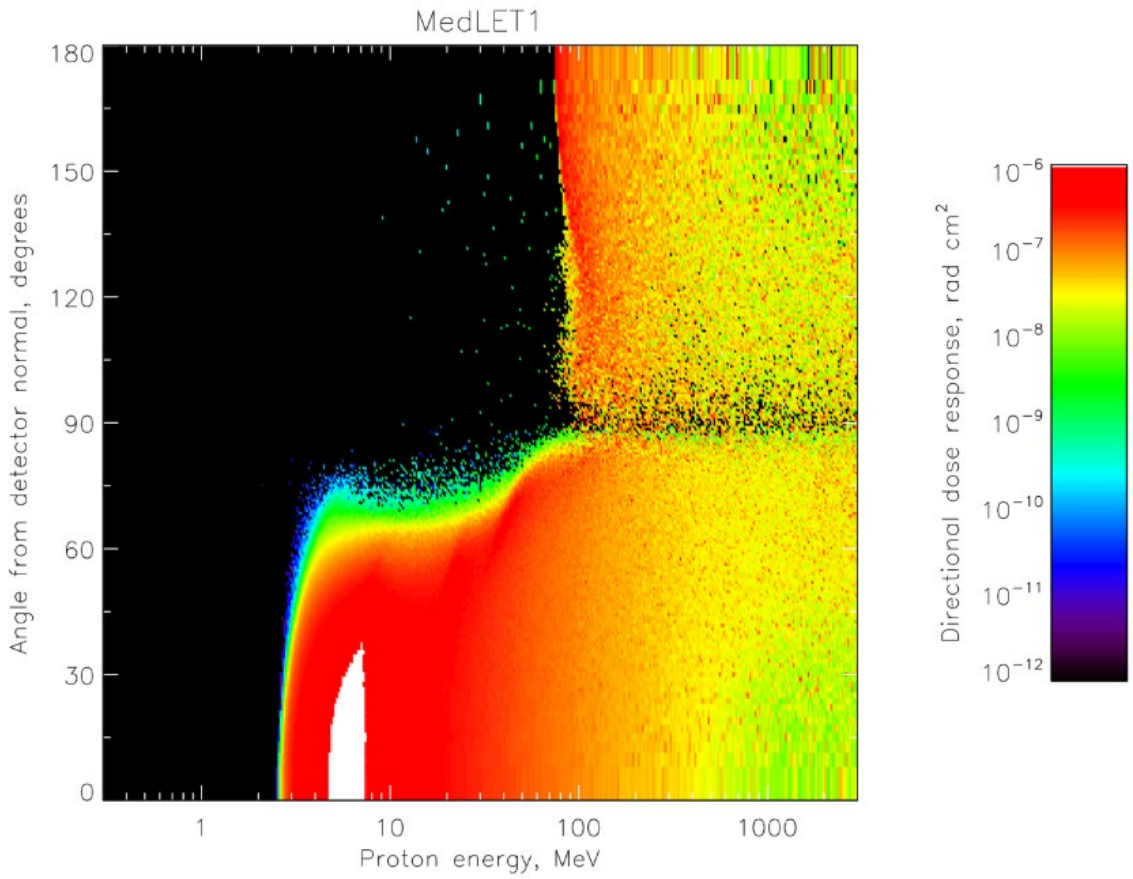

Figure 18. Directional dose response of MedLET1 to protons.

Figure 18 shows the directional dose response of MedLET1 to protons. The increase in angular width at about 40 MeV (with a fainter one barely visible around 25 MeV) marks energies at which protons start to be able to penetrate the aluminum around the 2.6 mil window, which is thicker than the window but not the full 300 mil wall thickness, as can be seen for the physically identical HiLET in Figure 4. As is the case for LoLET in Figure 16, penetration of the 300 mil walls from all sides starts at about 80 MeV.

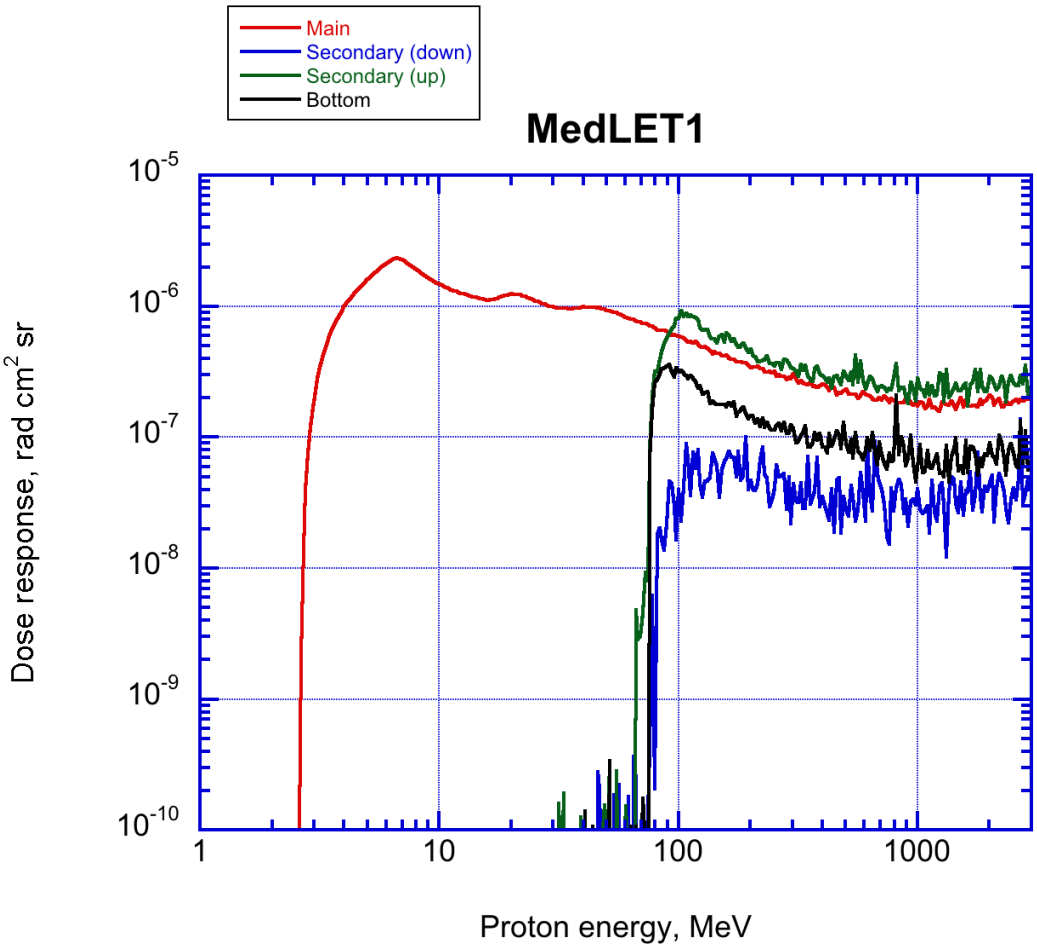

Figure 19. Omnidirectional dose response of MedLET1 to protons.

Figure 19 shows the omnidirectional dose response of MedLET1 to protons, again broken out by subsets of the incident trajectories. As is the case for LoLET in Figure 17, we see that the penetrating background is concentrated in the upgoing contribution represented by the green and black lines, which can be ignored for an ECP-Lite unit mounted on a large spacecraft.

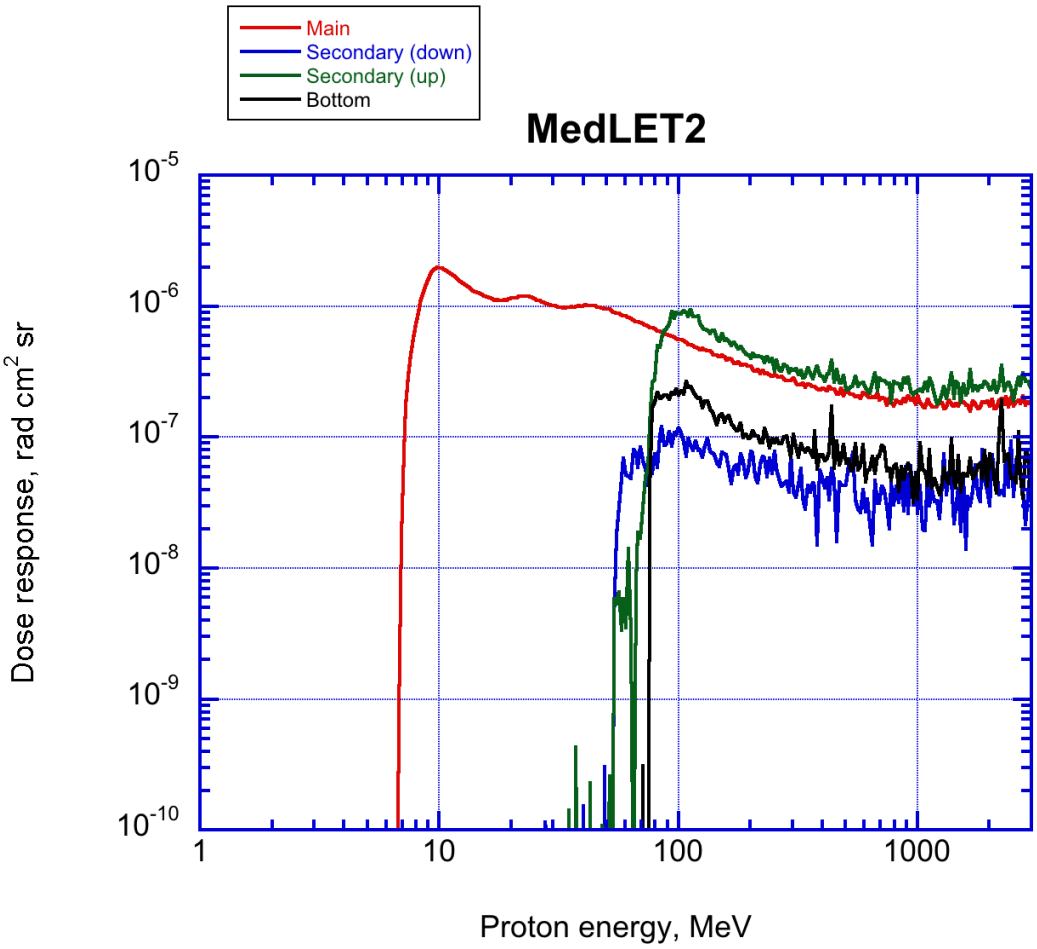

Figure 20. Omnidirectional dose response of MedLET2 to protons.

As is the case for electrons, the directional dose responses to protons of the four MedLET microdosimeters are similar except for a threshold energy that rises with window thickness, so we only show the omnidirectional dose plots for the other three. Figure 20 shows this for MedLET2, with features similar to the plot for MedLET1 in Figure 19.

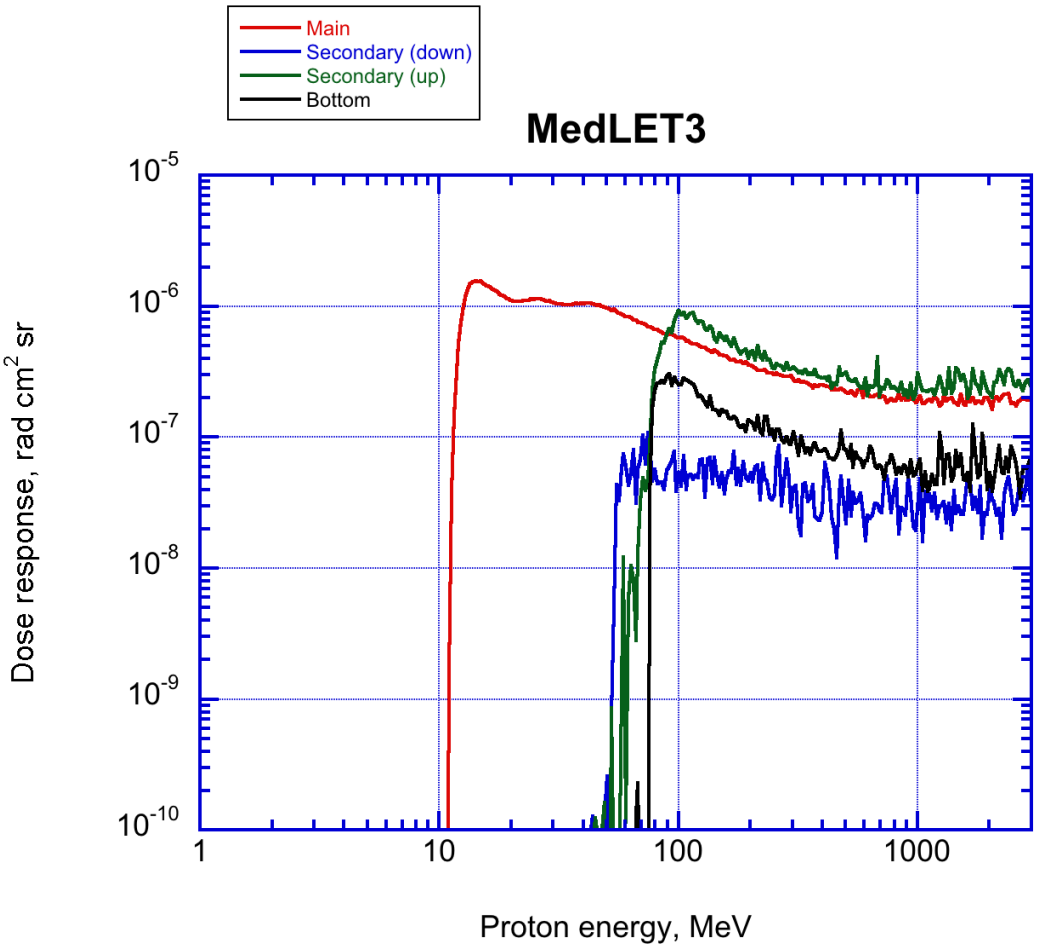

Figure 21. Omnidirectional dose response of MedLET3 to protons.

Figure 21 shows the omnidirectional dose response of MedLET3 to protons, again looking very similar to that of MedLET1 and MedLET2.

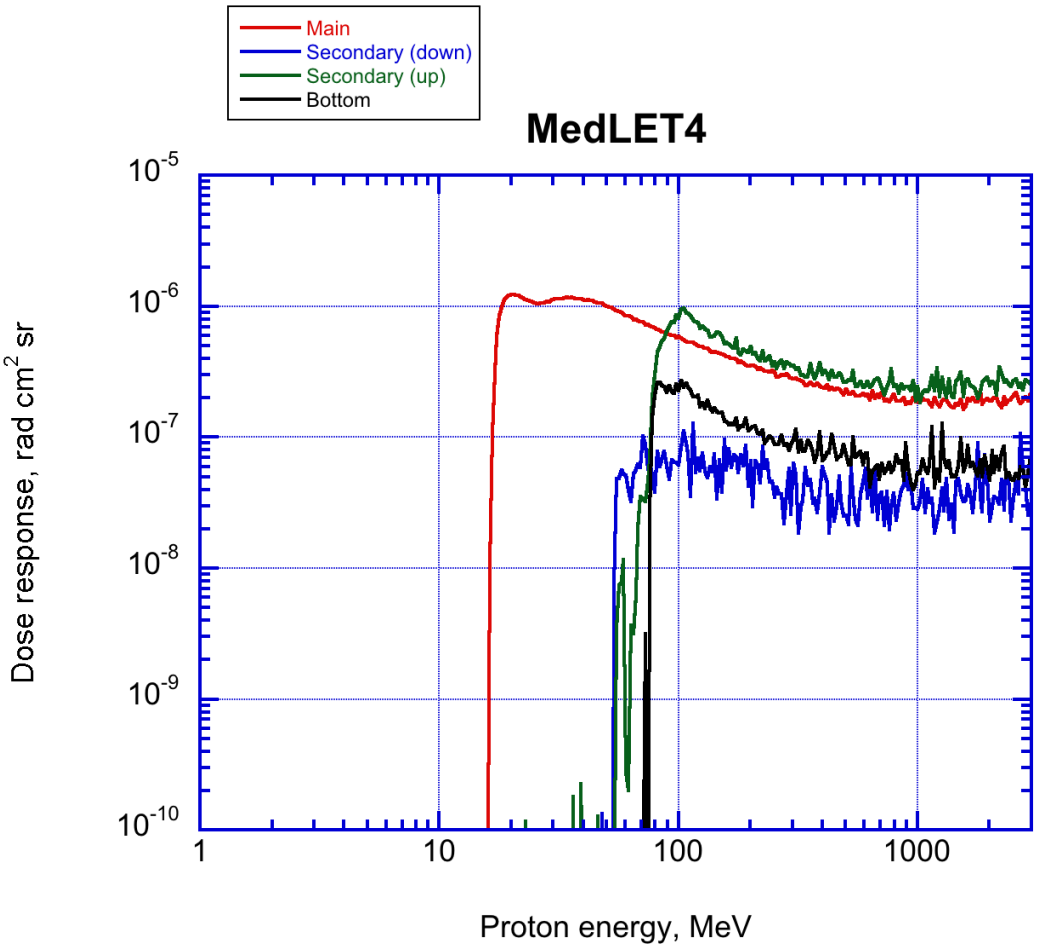

Figure 22. Omnidirectional dose response of MedLET4 to protons.

Figure 22 shows the omnidirectional dose response of MedLET4, with the thickest window and thus the highest energy threshold, to protons.

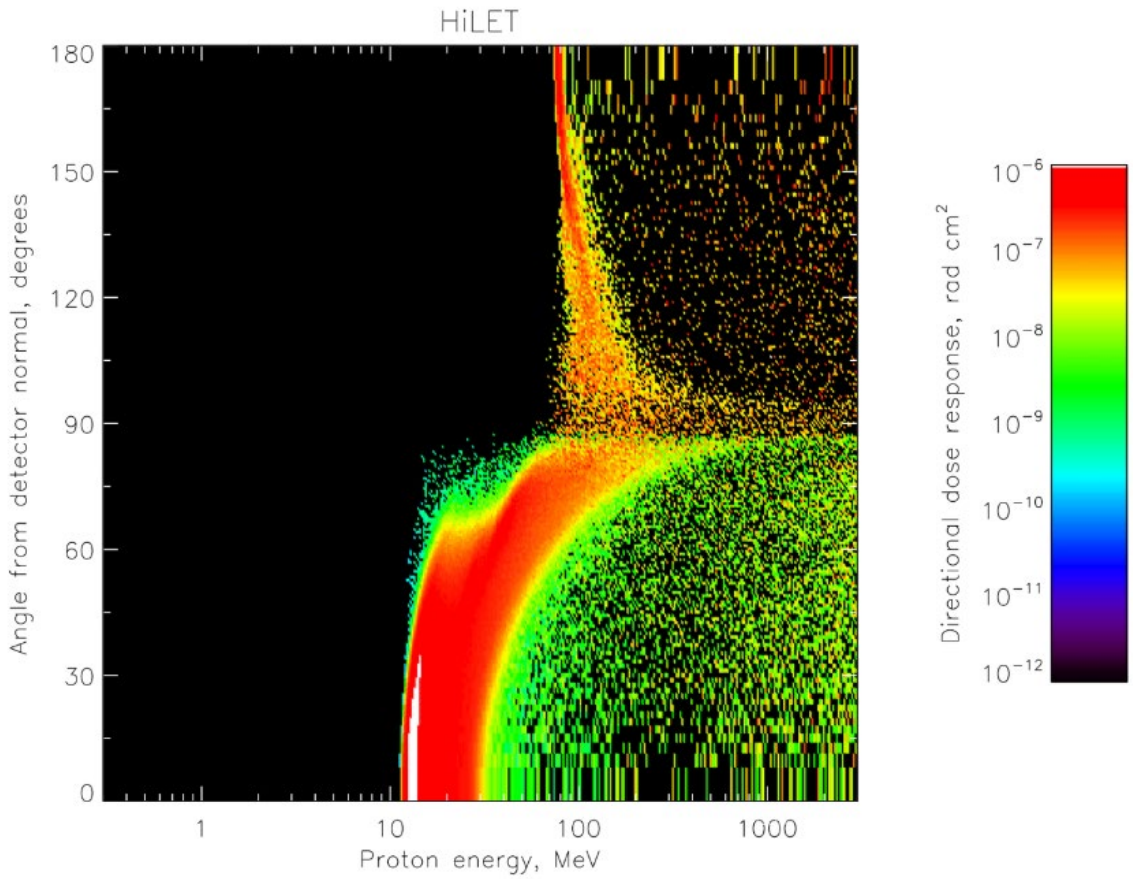

Figure 23. Directional dose response of HiLET to protons.

Figure 23 shows the directional dose response of HiLET to protons. At lower energies it is very similar to that of MedLET3 (not shown), which has a similar window thickness, but as the LET of protons drops with increasing energy their energy deposit starts to fall below the higher threshold of HiLET and so the high-energy response is greatly diminished.

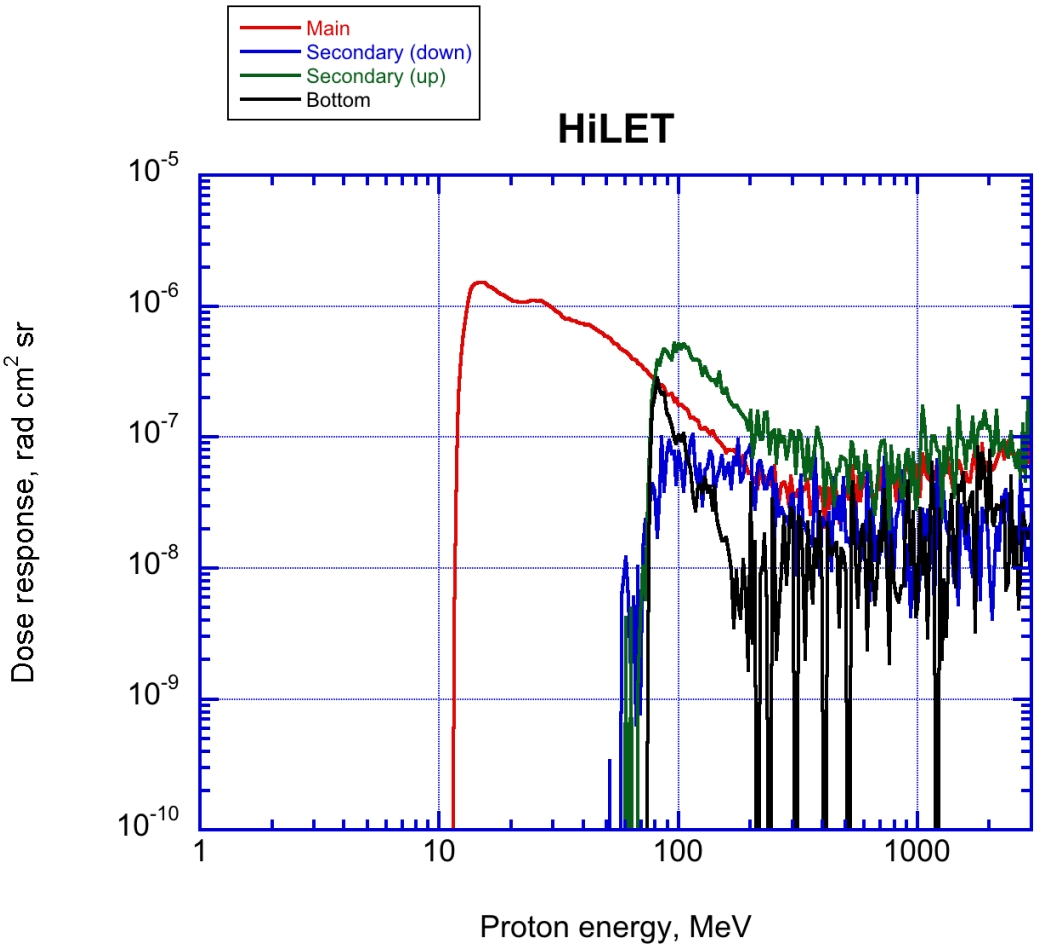

Figure 24. Omnidirectional dose response of HiLET to protons.

Figure 24 shows the omnidirectional response of HiLET to protons. The similarities to and differences from the MedLET3 response as described above are seen in comparing this figure with Figure 21 for MedLET3.

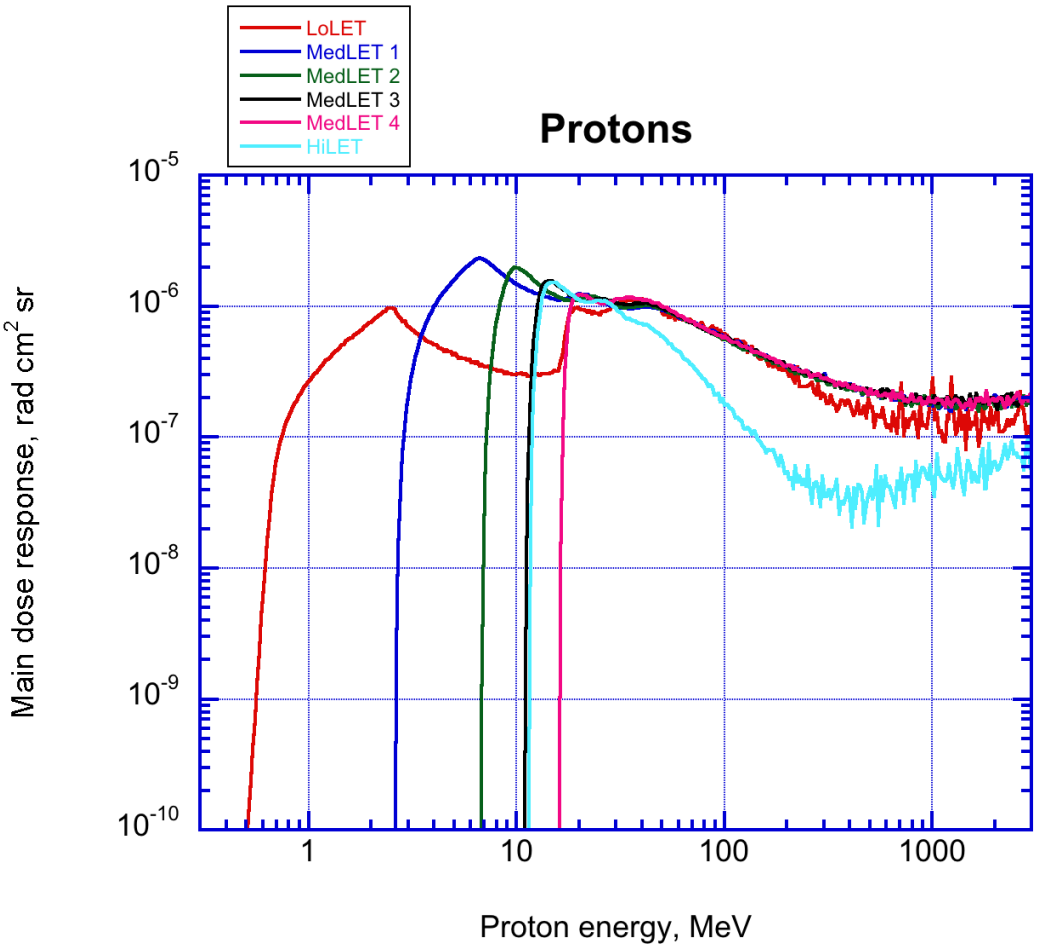

Figure 25. Omnidirectional dose response of all microdosimeter units to protons, into and near their apertures/windows.

Finally, Figure 25 shows the main component of the omnidirectional proton response in all six microdosimeters (red curves in Figures 17, 19-22, and 24). The high-energy responses of the four MedLET units are indistinguishable, as expected, with the HiLET response dropping as discussed above. The thin detector of LoLET means that, even with its lower electronic threshold (see Table 1), it also rejects some very energetic protons, as can be seen with a close examination of the differences between the directional dose responses at high energies for LoLET in Figure 16 and MedLET1 in Figure 18.

The full set of simulation results for protons and electrons, tabulated event by event, is being prepared so that we may derive energy thresholds and flux conversion factors that summarize the response of each microdosimeter for use in extraction of spectral information from flight data. The bowtie analysis technique as used for the similar REACH microdosimeters by O'Brien et al. [2] will be employed for this task.

4. References

[1] Allison, J., et al. (2016), "Recent Developments in Geant4," *Nucl. Inst. and Meth. In Phys. Res. A*, **835**, 186-225, doi: 10.1016/j.nima.2016.06.125

[2] O'Brien, T. P., M. D. Looper, and J. E. Mazur (2019), "REACH Dosimeter Equivalent Energy Thresholds and Flux Conversion Factors," Aerospace Corporation TOR-2019-02016

AEROSPACE REPORT NO.
TOR-2020-01640

Geant4 Simulations of ECP-Lite Microdosimeter Response to Electrons and Protons

Approved Electronically by:

James L. Roeder, DIRECTOR
SPACE SCIENCES DEPARTMENT
SPACE SCIENCE APPLICATIONS LABORATORY
ENGINEERING & TECHNOLOGY GROUP

Cognizant Program Manager Approval:

Peter A. Cunningham, SYSTEMS DIRECTOR
SPACE PROJECTS
DEVELOPMENTAL PROTOTYPES AND PROJECTS
DEFENSE SYSTEMS GROUP

Aerospace Corporate Officer Approval:

Martin Whelan, SR VP DEF SYS
DEFENSE SYSTEMS GROUP

Content Concurrence Provided Electronically by:

Mark D. Looper, RES SCIENTIST
MAGNETOSPHERIC & HELIOSPHERIC SCIENCES
SPACE SCIENCES DEPARTMENT
ENGINEERING & TECHNOLOGY GROUP

SY0633